Available online at www.sciencedirect.com
ScienceDirect
Journal of Catalysis 243 (2006) 292–302
JOURNAL OF CATALYSIS
www.elsevier.com/locate/jcat

Influence of the preparation method on the hydrotreating activity of MoS_2/Al_2O_3 extrudates: A Raman microspectroscopy study on the genesis of the active phase

Jaap A. Bergwerff [a], Marcel Jansen [b], Bob (R.) G. Leliveld [b], Tom Visser [a], Krijn P. de Jong [a], Bert M. Weckhuysen [a,*]

[a] *Inorganic Chemistry and Catalysis, Department of Chemistry, Utrecht University, Sorbonnelaan 16, 3508 TB Utrecht, The Netherlands*
[b] *Albemarle Catalysts BV, Nieuwendammerkade 1-3, 1022 AB Amsterdam, The Netherlands*

Received 8 May 2006; revised 7 July 2006; accepted 21 July 2006

Available online 14 September 2006

Abstract

Raman microspectroscopy was used to study the preparation of industrial MoS_2/Al_2O_3 extrudates. Using this technique, the influence of the impregnation solution composition on the nature and macrodistribution of Mo complexes inside these catalyst bodies was evaluated during their preparation process (impregnation, drying, and calcination). It was found that poor dispersion of the MoO_x phase in the calcined samples can be brought about by the formation of bulk $(NH_4)_3[Al(OH)_6Mo_6O_{18}]$ during impregnation or redistribution of Mo complexes during drying. The formation of crystalline MoO_3 and $Al_2(MoO_4)_3$ in the oxidic precursors leads to a poorly dispersed MoS_2 phase in the final catalyst and significantly lower hydrodesulfurization activity. The spatially resolved information that can be obtained, and its inherent sensitivity for the detection of crystalline phases make Raman microspectroscopy a powerful characterization technique for studying the preparation of industrial supported metal oxide catalysts.

Keywords: Hydrodesulfurization; Raman spectroscopy; Microspectroscopy; MO/Al_2O_3; Extrudates; Catalyst preparation

1. Introduction

To obtain transportation fuels, crude oil fractions are exposed to several hydrotreating steps to remove S-, N-, and metal-containing compounds in refineries [1]. Due to increasingly strict regulations, research has been dedicated to the preparation of more active catalytic systems for this process. Despite the development of alternatives, such as noble-metal catalysts [2], unsupported bulk MoS_2 catalysts [3,4] and supported metal–phosphide systems [5,6], supported $(Co/Ni)MoS_2$ catalysts are still predominantly used in most refineries, and their preparation remains an important industrial process. Throughout the years, numerous studies have been carried out to determine the influence of different preparation parameters on the structure and activity of these important catalysts [7–13]. However, the translation from recipes for the laboratory-scale preparation of the optimal supported catalyst to industrial-scale catalyst preparation is less well documented in the open literature. Specific problems can arise when the support is changed from powders to extrudates [14–16], whereas temperature and concentration profiles across catalyst beds often make large-scale preparation difficult to control.

For decades, Raman spectroscopy has been an important technique for characterizing supported oxide catalysts [17–19]. More recently, Raman microscopy has also found its way into heterogeneous catalysis research. The spatial resolution obtained in this way has, for instance, been exploited to follow the spreading of MoO_3 on an Al_2O_3 surface [20,21], monitor regions of different crystallinity in MoVW mixed-oxide catalysts [22], and study the reaction of molecules on catalytic surfaces [23] or even individual metal particles [24]. In recent years, Raman microspectroscopy [25] and other spatially resolved spec-

* Corresponding author. Fax: +31 302511027.
E-mail address: b.m.weckhuysen@chem.uu.nl (B.M. Weckhuysen).

0021-9517/$ – see front matter
doi:10.1016/j.jcat.2006.07.022

troscopic techniques, such as UV–vis microspectroscopy [26] and magnetic resonance imaging [27], have been applied to monitor the phenomena occurring during the preparation of mm-scale supported catalyst bodies. The application of these tools provides new opportunities to study the physicochemical processes occurring during the preparation of supported catalyst bodies and allow for better control of the dispersion and distribution of the active phase.

A previous study showed how Raman microspectroscopy can be applied to study the impregnation of Mo^{6+} solutions onto 3-mm Al_2O_3 pellets [25]. A strong interaction between Mo complexes and the Al_2O_3 support was found to lead to the formation of a $[Al(OH)_6Mo_6O_{18}]$ precipitate or the occurrence of Mo concentration gradients inside the impregnated pellets. In the current study, the technique is applied to monitor the nature and macrodistribution of the MoO_x phase in 1.5-mm Mo/Al_2O_3 extrudates during preparation. In this way, the implications of the processes described above on the nature and activity of the final MoS_2 phase can be evaluated. At the same time, the applicability of Raman microspectroscopy in studying the preparation of smaller catalyst extrudates can be put to the test.

A series of catalysts was prepared using $(NH_4)_6Mo_7O_{24}$-(AHM) as the Mo precursor salt. The influence of pH of the impregnation solution and the addition of citric acid as a complexing agent on Mo speciation in the extrudates after impregnation, drying, and calcination was evaluated. The formation of crystalline phases can result from either the formation of bulk $(NH_4)_3[Al(OH)_6Mo_6O_{18}]$ during impregnation or redistribution of the Mo phase during drying. Both phenomena can be prevented by the addition of citric acid to the impregnation solution. Subsequently, the activity of the different samples in the hydrotreatment of a light gas–oil (LGO) feed was tested. A correlation is found between the dispersion of the MoO_x phase in the calcined catalysts, the dispersion of the MoS_2 phase under reaction conditions, and the hydrodesulfurization (HDS) activity of the different catalyst samples.

2. Experimental

Pore volume impregnation was carried out on 20-g batches of cylindrical γ-Al_2O_3 extrudates (1.5 mm diameter and 10–15 mm long). A 5% excess of solution was used in all cases to ensure complete wetting of all extrudates. The pore volume of this support was 0.86 ml/g, and its surface area was 245 m^2/g. After impregnation, the wet samples were left for 1 h in a closed container before drying, which was done by passing hot air over the catalyst bodies. Drying was considered complete when the temperature of the catalyst bed reached a temperature of 120 °C. During aging and drying, the extrudates were kept in constant motion by rotation of the impregnation vessel. The dried extrudates were heated to 500 °C at a rate of 5 °C/min and calcined at this temperature for 1 h in stagnant air.

Two series of Mo/Al_2O_3 catalysts were prepared using Mo solutions with concentrations of 1.3 M and 1.8 M Mo, yielding theoretical MoO_3 loadings in the calcined catalyst of 14.5 wt% and 19.0 wt%, respectively. Within each series, impregnation was carried out with three AHM (Acros, p.a.) solutions of varying compositions. Besides AHM solutions at their natural pH of 6, basic AHM-solutions (pH 9) were prepared by adding 25 aqueous wt% NH_4OH solution (Baker, p.a.). A solution containing Mo–citrate complexes was prepared by adding citric acid (Merck, p.a.) in a Mo:citric acid ratio of 1:1. The effect of aging was studied in the case of the Mo–citrate solutions, where the aging step was omitted in an additional experiment and drying began immediately after impregnation. The codes for the different catalysts and procedures used for their preparation are summarized in Table 1.

Table 1
Preparation parameters and MoO_3 loading of the different samples used in this study

Sample code	Mo conc. (M)	Citrate conc. (M)	pH	Ageing time (h)	MoO_3 loading (wt%)
1.3Mo-pH 6	1.3	0	6	1	13.5
1.3Mo-pH 9	1.3	0	9	1	14.5
1.3Mo–citrate-l	1.3	1.3	0.5	1	14.5
1.3Mo–citrate-s	1.3	1.3	0.5	–	14.6
1.8Mo-pH 6	1.8	0	6	1	18.7
1.8Mo-pH 9	1.8	0	9	1	19.1
1.8Mo–citrate-l	1.8	1.8	0.5	1	19.0
1.8Mo–citrate-s	1.8	1.8	0.5	–	19.1

For Raman microspectroscopy measurements, Mo/Al_2O_3 extrudates were bisected and spectra recorded on the resulting cross-section, with no additional treatment. The roughness of the thus-created surface means that the total intensity of the inelastically scattered light varies when measurements are carried out at different positions on the sample. For presentation purposes, all spectra are therefore scaled to the fluorescence background. A Kaiser RXN spectrometer equipped with a 785-nm diode laser was used in combination with a Hololab 5000 Raman microscope. A 10× objective was used for beam focusing and collection of scattered radiation, resulting in a spot size on the sample of approximately 50 μm. The Raman laser power on the sample was approximately 10 mW. Care was taken to prevent beam damage by comparing the spectra thus obtained to spectra obtained with lower laser power. X-ray fluorescence (XRF) and X-ray diffraction (XRD) analyses were performed on crushed extrudates after calcination. XRD measurements were carried out on a Bruker-AXS D8 Advance powder X-ray diffractometer, equipped with automatic divergence slit and a Våntec-1 detector. The radiation source was cobalt $K\alpha_{1,2}$ ($\lambda = 1.79026$ Å, 30 kV, and 45 mA). To determine the distribution of Mo over the calcined extrudates, a scanning electron microscopy (SEM) study was preformed in combination with energy-dispersive analysis of X-rays (EDX). Samples were embedded in Castoglas and polished on SiC paper with 2-propanol. Samples were then carbon-coated, and line scans were recorded across the cross-section of bisected extrudates with a step size of 10 μm at a 20-kV acceleration voltage.

To determine the Mo loading at which the dispersion limit is reached and bulk MoO_3 begins to form on the surface of the particular γ-Al_2O_3 used in this study, a series of Mo/Al_2O_3 samples with different Mo loadings was prepared. Toward this

Table 2
Properties of the light gas oil used in the hydrotreatment tests

Sulfur (wt%)	1.2
Nitrogen (ppm wt)	102
Mono aromatics (wt%)	16.5
Di aromatics (wt%)	11.0
Di + aromatics (wt%)	0.8
Total aromatics (wt%)	28.3
Distillation (°C)	
Initial boiling point	178.4
10 vol%	224.0
30 vol%	261.4
50 vol%	283.8
70 vol%	309.3
90 vol%	347.8
Final boiling point	372.0

end, impregnation was carried out on a 150–500 μm sieve fraction of crushed extrudates, using AHM and equimolar Mo (ex AHM):citric acid solutions with Mo concentrations of 1.2, 1.4, 1.6, 1.8, and 2.0 M. These samples were dried at 120 °C and calcined at 500 °C for 6 h. Raman spectra were recorded on the calcined samples.

The catalytic activity of the different extrudates was evaluated in the hydrotreatment of a light gas–oil fraction. Characteristics of the feedstock are given in Table 2. A 5.9-g sample of each catalyst was loaded into a multitubular setup in which 10 catalyst samples can be tested simultaneously. Reaction was carried out at a weight hourly space velocity (WHSV) of 1.7 $g_{feed}\, g_{cat}^{-1}\, h^{-1}$, a H_2/oil ratio of 200 Nl $(H_2)/l_{feed}$, and a total pressure of 60 bar. The sulfur content of the oil was determined after reaction at 345, 360, and 375 °C using XRF for samples containing >0.06 wt% S and UV-detection for samples containing <0.06 wt% S. The relative error in these measurements is <2%. Sulfidation of the catalysts was carried out at 345 °C by adding dimethyldisulfide (DMDS) to the oil stream. After reaction, the catalyst samples were unloaded and stored in oil to prevent reoxidation.

For TEM analysis on the MoS_2/Al_2O_3 extrudates, whole extrudates were rinsed with toluene to remove the oil and vacuum-impregnated with the standard mixture Ultra-Low Viscosity Kit, hard version (Polaron Instruments). The mixture was transferred into a polyethylene capsule (BEEM) and mixed with fresh embedding medium. The epoxy embedding medium was hardened for at least 48 h under N_2 (0.2 MPa, 338 K). Sections of about 60 nm thickness were prepared using a Leica Reichert Ultracut-S ultramicrotome. Shortly after preparation, the sections were investigated with a JEOL JEM-2010F-HR TEM, with a 200-keV electron beam (Field Emission Gun, FEG). SEM analyses were performed on bisected embedded MoS_2/Al_2O_3 extrudates with a Leo Gemini 1550 SEM (Field Emission Gun), equipped with an Oxford INCA EDX system. EDX analysis was performed at 15 keV. To check for any possible reoxidation, Raman microspectroscopy was carried out on these samples as well.

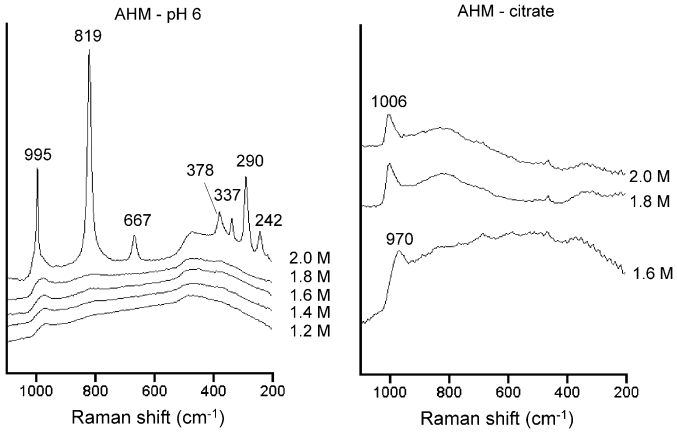

Fig. 1. Raman spectra recorded on calcined Mo/Al_2O_3 powder samples prepared from AHM-pH 6 (left) and AHM–citrate (right) solutions of different concentration.

3. Results and discussion

3.1. Mo/Al_2O_3 powder catalysts

Mo/Al_2O_3 and other supported metal-oxide catalysts are often referred to as monolayer systems, due to the tendency of the active phase to spread over the support at elevated temperatures [28]. In this way, an overlayer containing an amorphous MoO_x phase is formed on the support surface, and the surface free energy of the system is minimized. Thermodynamics dictate that bulk MoO_3 is only formed when the Al_2O_3 surface is completely covered. The Raman spectra of powdered Mo/Al_2O_3 samples prepared from AHM-pH 6 and AHM–citrate solutions of different concentration are shown in Fig. 1. For the AHM-pH 6 samples, an amorphous MoO_x phase can be seen in the samples prepared from 1.2–1.8 M Mo solutions, corresponding to 12–19 wt% MoO_3 in the final catalyst. A broad band at ∼980 cm^{-1} is observed in the Raman spectra recorded on these samples. The sample prepared from a 2.0 M Mo AHM-pH 6 solution (21 wt% MoO_3) clearly contained bulk MoO_3; intense bands at 995, 819, 667, 378, 337, 290, and 242 cm^{-1} were present in the spectrum [19]. Apparently, saturation coverage was reached at a MoO_3 loading of 19–21 wt%, corresponding to a theoretical surface coverage of 4.0–4.4 Mo atoms nm^{-2}, in good agreement with values reported in the literature [18,19]. Note that for preparation of the Mo/Al_2O_3 extrudates, 1.3 and 1.8 M Mo solutions were used, resulting in an overall MoO_3 loading below the dispersion limit. In other words, the total Al_2O_3 surface present in the extrudates should be sufficient to accommodate all Mo in an amorphous MoO_x phase. In contrast to the AHM-pH 6 samples, no bulk MoO_3 was detected in any of the AHM–citrate samples, even when a 2.0 M Mo solution was used. The formation of an amorphous MoO_x phase was found in the sample prepared from a 1.6 M Mo solution, judging from the position of the band maximum at 970 cm^{-1}. At higher Mo loadings, a band at 1006 cm^{-1} was observed that is generally assigned to $Al_2(MoO_4)_3$ [29]. But the low intensity and broadness of this band suggest that this is not a crystalline phase.

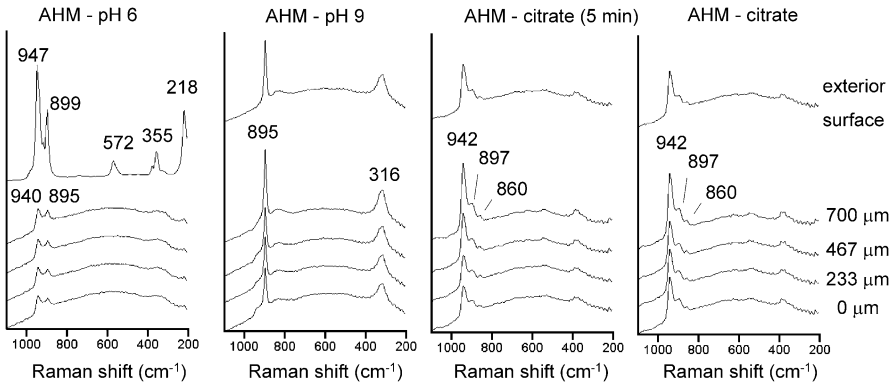

Fig. 2. Raman spectra recorded on bisected extrudates, 1 h after impregnation with 1.8 M AHM-pH 6, AHM-pH 9, and AHM–citrate solutions and 5 min after impregnation with a 1.8 M AHM–citrate solution. The distance of the measurement spot from the core of the extrudates is indicated on the right.

3.2. Impregnation of Al_2O_3 extrudates

The speciation of Mo^{6+}-complexes in AHM solutions at moderate pH is well established and can be easily monitored using Raman spectroscopy [19,30]. At the natural pH of AHM solutions (pH 5–6), $Mo_7O_{24}^{6-}$ is the predominant species, and the corresponding Raman spectrum exhibits bands at 940, 901, and 360 cm^{-1} [19,30]. At higher pH, MoO_4^{2-} is formed, as reaction (1) proceeds to the right. MoO_4^{2-} is the only complex present in the AHM-pH 9 solutions used in this study. Its Raman spectrum shows characteristic peaks at 895, 840, and 320 cm^{-1} [19,30]:

$$Mo_7O_{24}^{6-} + 4H_2O \leftrightarrow 7MoO_4^{2-} + 8H^+. \quad (1)$$

Raman spectra recorded on the bisected extrudates after impregnation with the different AHM solutions are presented in Fig. 2. After impregnation with the AHM-pH 6 solution, peaks at 895 and 940 cm^{-1} are observed for all positions inside the extrudates, which are superimposed on the fluorescence background, probably caused by impurities in the Al_2O_3 support. They demonstrate the presence of both MoO_4^{2-} and $Mo_7O_{24}^{6-}$ anions inside the Al_2O_3 pores. The formation of MoO_4^{2-} shows that the pH of the solution inside the Al_2O_3 was increased compared with the impregnation solution. This is caused by the protonation of basic hydroxyl groups on the Al_2O_3 surface. In the spectrum recorded on the outer surface, intense peaks at 947, 899, 572, 355, and 218 cm^{-1} indicate the presence of $Al(OH)_6Mo_6O_{18}^{3-}$ anions [31,32]. The observation of a white precipitate and the absence of a fluorescence background in the Raman spectrum indicate that an $Al(OH)_6Mo_6O_{18}^{3-}$ compound is covering the Al_2O_3 on the outside of the extrudates. The observation of bands at 895 and 316 cm^{-1} in spectra recorded throughout the wet extrudates shows that impregnation with the AHM-pH 9 solution leads to a homogeneous distribution of MoO_4^{2-} in the extrudates.

A whole range of different Mo–citrate complexes can be present in AHM–citric acid solutions. Stable complexes are documented in which the Mo:citrate ratio (2:1, 1:1, and 1:2), the number of Mo atoms (1, 2, and 4), and the protonation state varies with pH and concentration [33,34]. Formation constants, as reported in literature for these different complexes, have been determined using dilute solutions [34]. From calculations using these formation constants, $Mo_4(citrate)_2O_{11}^{4-}$ can be expected to be the predominant complex present in the AHM–citrate solutions used in this study [34]. It must be noted, however, that using these values to determine the constitution of the highly concentrated solutions is not without risk. The Raman spectrum of the impregnation solution shows bands at 942, 897, and 860 cm^{-1}. In the case of the AHM–citrate samples, measurements were also carried out directly after impregnation. In this way, the distribution of Mo complexes before the start of the drying process can be obtained for all Mo/Al_2O_3 samples described in this study. In all cases, peaks are observed exclusively at 942, 897, and 860 cm^{-1}, indicating that the $Mo_4(citrate)_2O_{11}^{4-}$ complex remained intact inside the Al_2O_3 pores after impregnation. Moreover the distribution of Mo complexes 5 min after impregnation seems to be homogeneous, judging from the constant intensity of the MoO_{2t} vibrations compared with the Al_2O_3 fluorescence background. In a previous study, the transport of this complex through the Al_2O_3 pore system was found to be slow, and a homogeneous distribution of $Mo_4(citrate)_2O_{11}^{4-}$ was found only 3 h after impregnation of 3-mm Al_2O_3 pellets with a 1 M Mo AHM–citrate solution [25]. This was attributed to the strong Coulomb interaction between the negatively charged Mo complexes and the Al_2O_3 surface, which is protonated due to the low pH of the impregnation solution. In this case, however, the concentration of the impregnation solution was higher, and the diameter of the extrudates was half that of the pellets used before. Both changes will favor a uniform distribution of Mo complexes. Apparently, this resulted in a homogeneous distribution of the Mo–citrate complexes within 5 min after impregnation despite the interaction between $Mo_4(citrate)_2O_{11}^{4-}$ and the Al_2O_3 surface.

3.3. Drying and calcination of Mo/Al_2O_3 extrudates

Formation of a layer of white powder on the external surface was observed by visual inspection of dried and calcined extrudates prepared from AHM-pH 6 solutions, regardless of Mo loading. In approximately 50% of all calcined AHM-pH 6 extrudates, areas of different color were also observed on the inside of these extrudates. Both phenomena are clearly visible in the SEM image in Fig. 3, which shows cross-sections

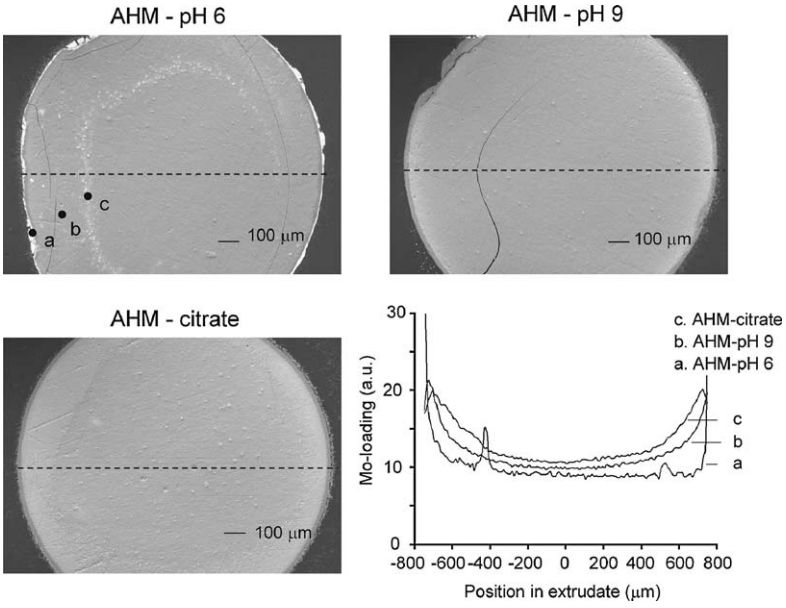

Fig. 3. SEM-images of bisected 19 wt% Mo/Al_2O_3 extrudates, prepared from AHM-pH 6, AHM-pH 9, and AHM–citrate solutions after calcination. The corresponding Mo-concentration profiles, derived from EDX measurements are also shown.

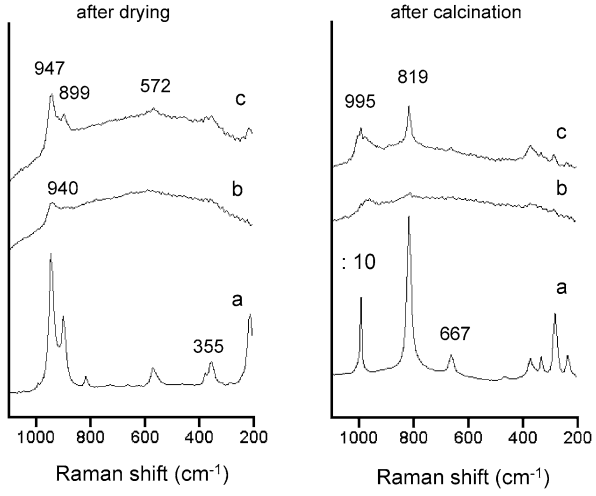

Fig. 4. Raman spectra recorded at different positions on bisected 19 wt% MoO_3/Al_2O_3 extrudates prepared from an AHM-pH 6 solution after drying (left) and calcination (right). Spectra are recorded on (a) external surface, (b) internal bulk of the extrudates, (c) inhomogeneities in the extrudates. Measurement positions are similar to the points labeled as a–c indicated in the SEM image in Fig. 3.

of calcined extrudates, prepared from different 1.8 M Mo solutions. A crust of white material and a ring of lighter color can be seen in the AHM-pH 6 sample, whereas the other extrudates are much more homogeneous. The corresponding EDX-linescans are also included in this figure. It can be seen that the Mo loading is much higher at the external surface and at the divergent spots on the inside of the AHM-pH 6 extrudate than in the rest of the sample. Raman spectra were recorded on similar positions in both dried and calcined catalyst bodies (labeled a, b, and c in the SEM image), as shown in Fig. 4. The crust on the outside of the dried catalyst bodies (a) consisted of $(NH_4)_3[Al(OH)_6Mo_6O_{18}]$, as indicated by the intense bands at 947, 899, 563, and 355 cm^{-1} [31,35]. This material was also present in areas with high Mo concentration on the inside of the extrudates (c), whereas $Mo_7O_{24}^{6-}$ complexes were present mainly in the bulk of the sample (b), as indicated by the position of the main MoO_{2t} vibration at 940 cm^{-1} [19].

The $(NH_4)_3[Al(OH)_6Mo_6O_{18}]$ phase formed during impregnation was clearly retained after drying. It formed due to the so-called "ligand-promoted dissolution" of the Al_2O_3 support [32], resulting from the complexation of Al^{3+} ions by oxomolybdate complexes under acidic conditions, as described in the following reaction:

$$6Mo_7O_{24}^{6-} + 7Al^{3+} + 24H_2O \rightarrow 7Al(OH)_6Mo_6O_{18}^{3-} + 6H^+. \quad (2)$$

The high Mo concentration present on the outside of the extrudates after impregnation allows for a chain reaction to occur. Al^{3+} ions are generated by dissolution of the support and consumed in the formation of $Al(OH)_6Mo_6O_{18}^{3-}$. The low solubility of this compound leads to the precipitation of $(NH_4)_3[Al(OH)_6Mo_6O_{18}]$. The Al^{3+} concentration in solution is thus kept low, and increasing amounts of Al_2O_3 are dissolved as a layer of $(NH_4)_3[Al(OH)_6Mo_6O_{18}]$ is formed [32]. Inside the pores of the Al_2O_3, toward the inside of the extrudates, the pH of the solution increased due to the buffering action of the support, and MoO_4^{2-} instead of $Al(OH)_6Mo_6O_{18}^{3-}$ complexes were formed. Apparently, in certain domains inside the extrudates, circumstances after impregnation are similar to those found on the exterior of the extrudates, and formation of the heteropolyanions occurs. These domains could consist of cracks in the extrudates or areas of low-density Al_2O_3 created during the extrusion process. At these positions, the amount of $Mo_7O_{24}^{6-}$ anions per unit Al_2O_3 surface area is high, and the buffering effect of the support is not sufficient to prevent the formation of bulk $(NH_4)_3[Al(OH)_6Mo_6O_{18}]$.

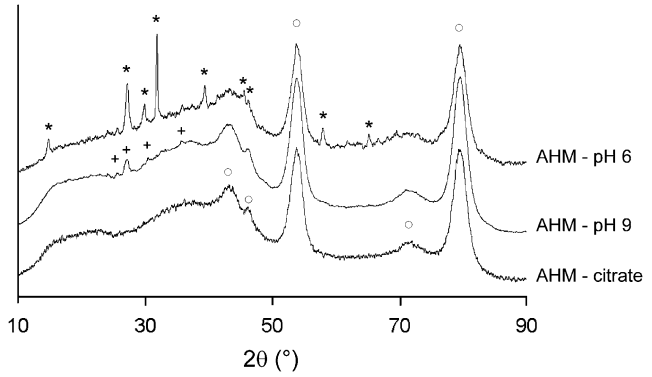

Fig. 5. XRD patterns recorded on crushed 19 wt% MoO_3/Al_2O_3 extrudates after calcination, prepared from different AHM solutions. Reflections corresponding to the presence of crystalline γ-Al_2O_3 (○) (ICDD 48-0367), MoO_3 (⋆) (ICDD 5-508), and $Al_2(MoO_4)_3$ (+) (ICDD 23-764) are indicated.

In general, the nature of Mo complexes present in dried Mo/Al_2O_3 catalysts under ambient conditions is a function of the Mo loading and the nature of the support [36]. The same complexes can be formed on the hydrated Al_2O_3 surface and in solution. Just as the pH of a solution determines the speciation of Mo complexes in a solution, the point of zero charge (PZC) of the hydrated surface layer determines which Mo complexes are present. The value of the PZC of the total surface is a result of the individual PZC values of bulk Al_2O_3 (∼9) and the AHM (∼6) deposited on the surface [37]. Hence the PZC of a Mo/Al_2O_3 system will decrease with increasing Mo loading. Consequently, at the high Mo loadings used in this study, the PZC of the system will be close to 6, and $Mo_7O_{24}^{6-}$ entities are present predominantly in the bulk of the dried material. Furthermore, drying results in a concentration of Mo complexes on the surface, also favoring $Mo_7O_{24}^{6-}$ formation.

As shown in Table 1, XRF measurements showed that the total MoO_3 loading in the calcined catalysts was largely unaffected by the preparation method. After calcination, sharp peaks at 995, 819, 667, 378, 337, 290, and 242 cm^{-1} occur in the Raman spectra recorded on calcined AHM-pH 6 samples for positions showing the presence of $(NH_4)_3[Al(OH)_6Mo_6O_{18}]$ after drying. On calcination, the $(NH_4)_3[Al(OH)_6Mo_6O_{18}]$ agglomerates were converted into bulk MoO_3 in accordance with the literature [35]. The formation of bulk MoO_3 is also observed in the XRD pattern recorded on crushed 19 wt% MoO_3 AHM-pH 6 extrudates, shown in Fig. 5. In this pattern, all main diffraction lines of orthorhombic MoO_3 [$2\theta = 14.9°$ (6.99 Å), 27.2° (3.80 Å), 30.0° (3.45 Å), 31.8° (3.27 Å), 39.4° (2.65 Å), 58.0° (1.85 Å), and 62.2° (1.73 Å)] are observed along with the broad peaks originating from the γ-Al_2O_3 support [38]. In other areas, an amorphous MoO_x phase was detected and a broad band observed in the Raman spectra. As discussed earlier, at elevated temperature, bulk MoO_3 can be expected to spread over the Al_2O_3 support to form an amorphous MoO_x overlayer. Although the total Al_2O_3 surface area in the extrudates was sufficient to accommodate all Mo present in the system in an amorphous overlayer, the creation of areas with a high Mo concentration led to formation of bulk MoO_3. Apparently, in mm-scale catalyst bodies, transport distances are too large for complete spreading of the MoO_3 over the support during calcination for 1 h, a calcination period typical for the industrial preparation of $(Ni/Co)Mo/Al_2O_3$ catalysts. Using a quantitative Raman spectroscopy method on crushed extrudates, the total amount of crystalline MoO_3 formed in the extrudates is estimated as $3(\pm1)$% of the total weight for both the 14 wt% and the 19 wt% MoO_3 samples. Details of the procedure used to obtain these values are given in Supplementary material.

On visual inspection, the calcined extrudates prepared from AHM-pH 9 solutions appear rather homogeneous. This can also be seen in the SEM image in Fig. 3. Nonetheless, an eggshell distribution of Mo can be seen in the corresponding EDX line scan. The Raman spectra recorded on these dried extrudates (shown in Fig. 6) indicate the presence of $Mo_7O_{24}^{6-}$ complexes throughout the extrudates, judging from the maximum in the spectra at 940 cm^{-1} for all positions inside the sample. Drying of the extrudates led to evaporation of excess ammonia from the solution and a decrease in the pH of the solution inside the pores of the Al_2O_3. Consequently, after drying, the composition on the interior of the extrudates was similar to that of the AHM-pH 6 sample, and $Mo_7O_{24}^{6-}$ formed, as was already discussed above. The eggshell distribution of Mo seen in the EDX line scan can also be inferred from the Raman measurements, as the intensity of the Mo–O stretch vibrations increases toward the outside of the extrudates after scaling to the Al_2O_3 fluorescence background. After calcination, an amorphous MoO_x phase was present throughout the 14 wt% MoO_3 extrudates prepared from the AHM-pH 9 solution. A broad band can be seen at 960–980 cm^{-1} for all positions. The same phase also was present near the core of the extrudates with the high Mo loading. However, in the 19-wt% MoO_3 sample, crystalline phases can be detected near the outer surface of the extrudates. A sharp peak at 1006 cm^{-1} reveals the presence of bulk $Al_2(MoO_4)_3$ in the outer 50 μm of the sample; bulk MoO_3 (995 and 819 cm^{-1}) was present at the exterior surface. The presence of crystalline $Al_2(MoO_4)_3$ also can be seen in an XRD pattern recorded on the corresponding crushed extrudates, with small peaks present at 2θ values of 25.8° (4.01 Å), 27.3° (3.78 Å), 30.4° (3.41 Å), and 35.8° (2.91 Å). An attempt to quantify the amount of crystalline material in this sample failed, as described in Supplementary material.

After impregnation with the AHM-pH 9 solution, the interaction between MoO_4^{2-} anions and the Al_2O_3 surface can be expected to be relatively weak. Because the pH of the impregnation solution is similar to the PZC of the support material, the Al_2O_3 surface will be neutrally charged, and the Coulomb interaction with the MoO_4^{2-} anions will be negligible. It is well known that the drying procedure can drastically influence the distribution of metal ion complexes in supported catalyst bodies, especially when a poor interaction exists between the metal ion precursor complexes and the support oxide after impregnation [14,15]. Thus, an eggshell distribution of Mo complexes is found in the AHM-pH 9 extrudates after drying. This particular distribution is often observed when catalyst bodies are dried at low rates. In this case, evaporation of water occurs at the periphery of the extrudates, and liquid is drawn from the center of the bodies toward the external surface. This transport can pro-

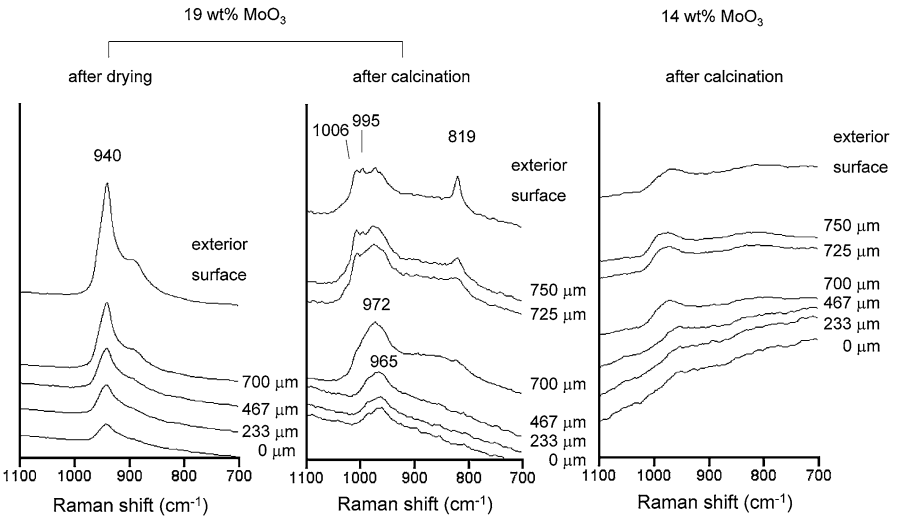

Fig. 6. Raman spectra recorded on bisected extrudates after drying (left) and calcination (right) of extrudates impregnated with 1.8 M and 1.3 M AHM-pH 9 solutions. The distance of the measurement spot from the core of the extrudates is indicated to the right of the spectra.

ceed via connected liquid elements, as well as through a film of liquid covering the walls of emptied pores. Dissolved metal ion precursor complexes travel with this flow of the liquid and when precipitation takes place, the liquid phase is primarily located in the outer layer of the catalyst bodies. When drying is complete, an eggshell distribution of the metal-ion salts remains [39]. A regime of slow drying can be expected to be operative when (relatively) large batches of impregnated support bodies are dried, as is the case in this study.

For the 19-wt% MoO_3 samples, due to the eggshell distribution, the Mo loading near the external surface of the extrudates exceeded the value required for the dispersion limit coverage. Hence, formation of crystalline Mo phases occurred after calcination. At low loadings, an eggshell distribution of Mo would be expected to be present as well. However, in this case, the macrodistribution of Mo is less crucial, because a slight eggshell distribution does not necessarily lead to loadings exceeding the dispersion limit coverage near the outside of the extrudates. An amorphous MoO_x phase is formed throughout the extrudates.

The Raman spectra recorded on the 19-wt% MoO_3 AHM–citrate samples after drying and calcination are presented in Fig. 7. For the dried sample, the peak positions of the main Mo–O vibrations are similar to those in the spectra recorded on the wet material. The $Mo_4(citrate)_2O_{11}^{4-}$ complex is preserved on the Al_2O_3 surface after drying. A slight Mo-concentration gradient is present, judging from the increased intensity of the Mo–O stretch vibration relative to the Al_2O_3 fluorescence background toward the outside of the extrudates. The Mo profile obtained from the EDX line scan (Fig. 3) supports this observation. The gradient is less pronounced compared with samples prepared from the AHM-pH 9 solution, because the interaction between the $Mo_4(citrate)_2O_{11}^{4-}$ complexes and the Al_2O_3 surface after impregnation is stronger. There was no difference in the spectra of the AHM–citrate-l and AHM–citrate-s samples; these samples already exhibited the same distribution of $Mo_4(citrate)_2O_{11}^{4-}$ before the drying process. After calcination,

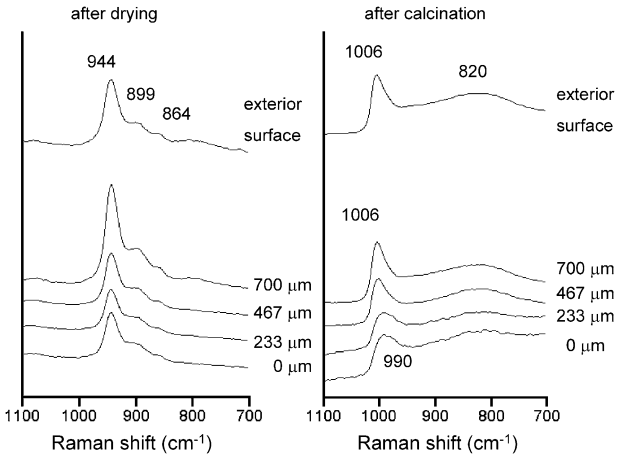

Fig. 7. Raman spectra recorded on bisected 19 wt% MoO_3/Al_2O_3 extrudates prepared from an AHM–citrate solution after drying (left) and calcination (right). The distance of the measurement spot from the core of the extrudates is indicated to the right of the spectra.

merely amorphous MoO_x phases were present in the catalysts, regardless of the MoO_3 loading. Relatively broad bands can be seen observed in the Raman spectra, and only reflections due to the γ-Al_2O_3 support are present in the XRD pattern recorded on the crushed extrudates (Fig. 5) [38]. The position of the Raman band shifted to higher frequency as the Mo loading increased toward the outside of the pellet. Near the external surface in the 19-wt% MoO_3 sample, the maximum of the band occurs at 1006 cm^{-1}. This band's position corresponds to the formation of an $Al_2(MoO_4)_3$ phase, whereas its broadness suggests the presence of an amorphous phase. Due to the eggshell distribution, the local Mo concentration near the external surface will exceed the value corresponding to the dispersion limit coverage derived from the measurements on AHM-impregnated powdered Al_2O_3. Nevertheless, as in the case of the powdered samples prepared from AHM–citrate solutions, no crystalline phases are observed. Apparently, more Mo can be accommodated in an amorphous $Al_2(MoO_4)_3$ phase

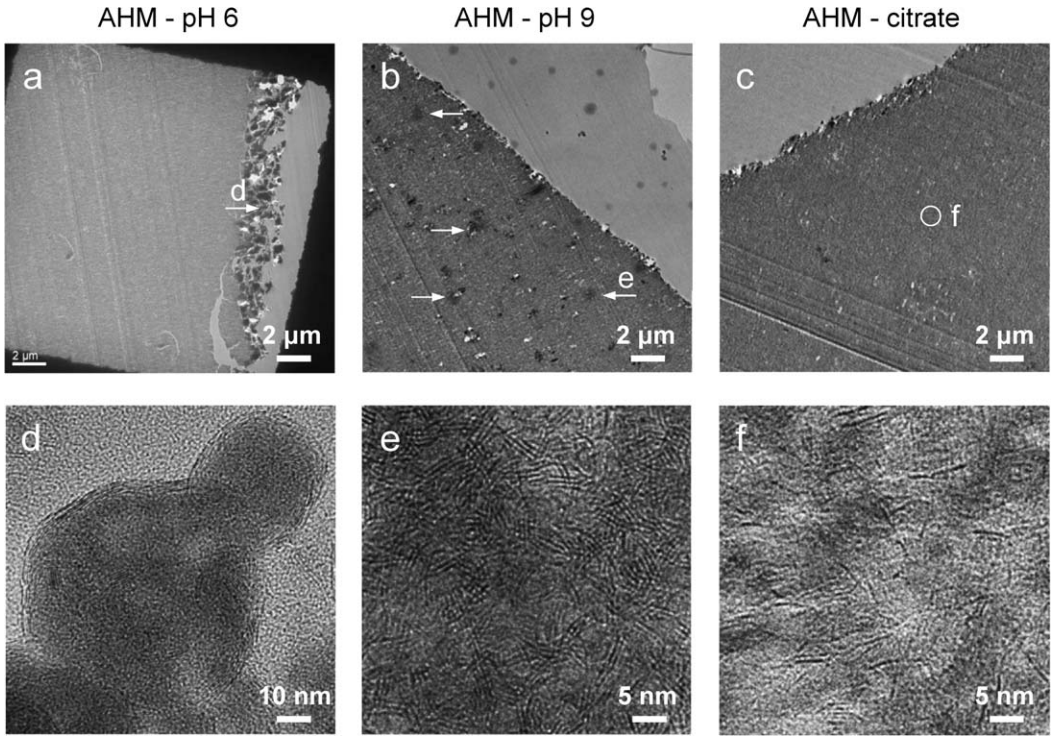

Fig. 8. TEM images recorded on embedded MoS_2/Al_2O_3 extrudate slices, prepared from different 19 wt% MoO_3 samples. Low-magnification images (a–c) were recorded near the external surface of the extrudates. The position where the high-magnification images (d–f) were recorded are indicated in images a–c.

on the Al_2O_3 surface when the preparation is started from an AHM–citrate solution.

3.4. Characterization of MoS_2/Al_2O_3 extrudates

Raman spectra recorded on the embedded extrudates after reaction merely showed bands at 226, 384, and 406 cm^{-1}, corresponding to the presence of MoS_2 for all positions in all samples under investigation [40]. The absence of any Mo–O stretch vibration bands in the 900–1000 cm^{-1} region indicates that sulfidation was complete and that reoxidation of the sample had not occurred to any significant extent during handling of the sulfidic catalysts. The Mo distributions obtained from SEM–EDX measurements on the MoS_2/Al_2O_3 extrudates were similar to the profiles recorded on the corresponding oxidic samples. In other words, sulfidation and reaction conditions had no noticeable influence on the macroscopic distribution of Mo in the extrudates.

TEM images recorded on different 19-wt% MoO_3 extrudate slices after reaction are shown in Fig. 8. The most striking differences in the three samples were found near the outside of the extrudates, as can be seen by comparing images a, b, and c. For the AHM-pH 6 sample, a ∼2-µm-thick layer of dense material can be seen on the external surface of the catalyst extrudates. The high-magnification micrograph recorded on this layer (image d) clearly shows that these particles contain MoS_2, because slabs are readily visible. In the AHM-pH 9 sample, areas of higher density (typically 200 nm) are observed in a 50-µm-thick ring on the outside of the extrudates. These areas are indicated by the arrows in image b. Images at higher magnification (image e) show that they consist of agglomerates of MoS_2 slabs. For the AHM–citrate sample, none of these features was observed, and the sample appeared to be homogeneous at low magnification. Well-distributed MoS_2 slabs were observed at higher magnification, as is illustrated in image f. Only a few double slabs and no multistacked slabs are found, indicating that the MoS_2 phase is in close contact with the support. Near the core of the extrudates, all samples show a well-dispersed MoS_2 phase, although with lower density due to the lower Mo concentration at these positions.

3.5. Activity of MoS_2/Al_2O_3 extrudates in LGO hydrotreatment

The HDS activities of the different MoS_2/Al_2O_3 extrudate samples are obtained from the conversion of sulfur-containing compounds. Values for the HDS weight activities (k_{WHSV}) for the different catalysts at different reaction temperatures are presented in the Arrhenius plot in Fig. 9. The relative HDS activities of the different samples at 360 °C, derived from the lines, are presented in Fig. 10. The HDS conversion was between 0.7 for the least active catalyst at 345 °C and 0.975 for the most active catalyst at 375 °C. Reaction rate coefficients (k_{WHSV}) were determined from the weight hourly space velocity (WHSV) and the total concentration of S-containing compounds in the feed before (C_{feed}) and after reaction ($C_{product}$), assuming a first-order reaction, using Eq. (3). Based on the relative error in the determination of the sulfur content (<2%), the relative error in the reaction rate constants was <1%. The LGO-feed had numerous different S-containing compounds, ranging from reactive thiophene derivates to substituted dibenzothiophenes, which are notoriously difficult to decompose [41]. Hence, the

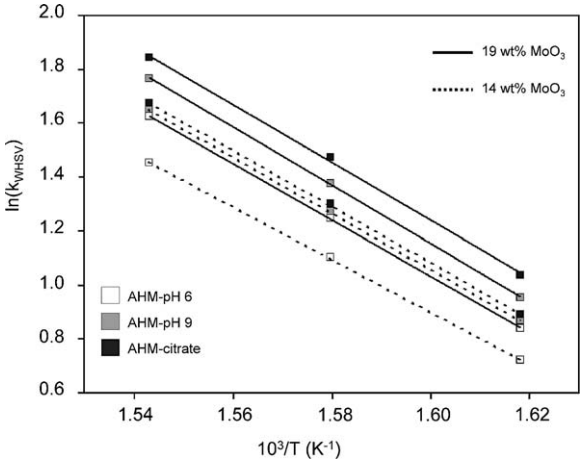

Fig. 9. Arrhenius plot ($\ln k_{\mathrm{WHSV}}/T^{-1}$) of the HDS reaction constants for the different catalysts.

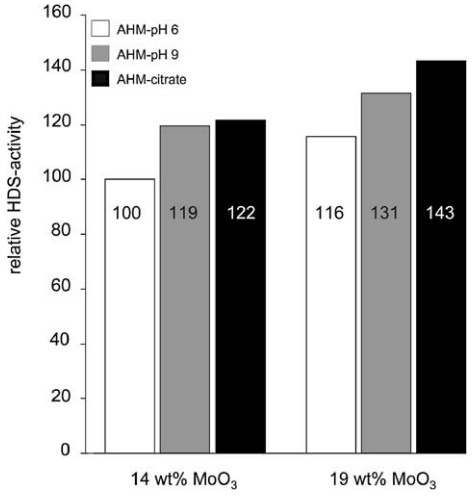

Fig. 10. Bar diagram showing the normalized HDS activities of the different catalysts, derived from the reaction rate constants (k_{WHSV}) at 360 °C.

constitution of the library of S-containing compounds and their average reactivity can change with conversion. However, the total S concentration is inevitably used for determining HDS activity.

Theoretically, this results in a decreasing apparent rate constant with increasing conversion and a decreasing observed reaction order from 2 to 1 [42]. Indeed, in the literature, a HDS reaction order between 1 and 2 was found when hydrotreatment was carried out on industrial feeds using (Ni/Co)Mo/Al_2O_3 catalysts [43–45]. For the specific catalysts, feeds, and conversion ranges used in this study, a reaction order of 1 was found to give the best correlation between $\ln(k_{\mathrm{WHSV}})$ and T^{-1}. A similar slope was found in the Arrhenius plots for the different catalysts. Apparently, the activity of the different catalysts is merely a function of the number of active sites. The average activation energy derived from the slopes of the lines in the Arrhenius plot was 87 kJ mol^{-1}:

$$k_{\mathrm{WHSV}} = \mathrm{WHSV}\ln\left(\frac{C_{\mathrm{feed}}}{C_{\mathrm{feed}} - C_{\mathrm{product}}}\right). \quad (3)$$

Samples prepared from AHM–citrate solutions showed the highest activity in all cases. The absence of any crystalline oxidic material after calcination and the presence of a well-dispersed MoS_2 phase throughout the extrudates explain these catalysts' superior performance. However, the activity was not completely proportional to the MoO_3 loading. Apparently, the higher MoO_3 loading caused a slightly lower dispersion of the MoS_2 phase. The low activity of the AHM-pH 6 samples can be explained by the formation of considerable amounts of bulk MoO_3 in specific areas of the extrudates, as observed on Raman microspectroscopy and XRD measurements. From TEM images, it is clear that on sulfidation, this phase was transformed into large MoS_2 clusters, expected to be mainly inactive in catalysis. The amount of crystalline MoO_3 formed in the AHM-pH 6 samples (3 ± 1 wt%) can be estimated as 21% for the 14-wt% MoO_3 sample and 15% for the 19-wt% MoO_3 sample. The AHM-pH 6 samples were 19% less active than the AHM–citrate samples of the same Mo loading. Considering the identical activation energy found for all catalysts, a semiquantitative correlation seemed to exist between the percentage of effective MoS_2 phase and the HDS activity.

At the low Mo loading, the catalyst prepared from an AHM-pH 9 showed a HDS activity comparable to that of the AHM–citrate sample. No crystalline phases were observed in the oxidic precursor for this sample. At the high Mo loading, however, the activity of the AHM-pH 9 sample was noticeably (9%) lower than that of the AHM–citrate catalyst. In this case, the formation of bulk MoO_3 and $Al_2(MoO_4)_3$ was observed in the outer shell of the oxidic extrudates, and MoS_2 clusters were visible in the TEM images recorded on the sulfidic material. Apparently, the poor dispersion of the MoS_2 phase rendered these clusters inactive in the HDS reaction.

3.6. Raman microspectroscopy in industrial catalyst preparation

It was found in this study that the speciation of Mo complexes in Mo/Al_2O_3 extrudates can be monitored using Raman microspectroscopy at all stages of catalyst genesis. Particularly in impregnated and dried samples, the sharp peaks due to the presence of individual hydrated Mo^{6+}-complexes provide detailed information about the nature of the Mo phase on the Al_2O_3 surface. The physicochemical processes occurring during the impregnation and drying step thus can be monitored in great detail. Transport rates of different Mo complexes through the Al_2O_3 pore system and their reaction with the Al_2O_3 surface can be envisaged [25,46,47]. The spatially resolved information obtained using Raman microspectroscopy sheds light on detrimental processes occurring during catalyst preparation. In this specific study, the formation of MoO_3 in calcined Mo/Al_2O_3 extrudates prepared from AHM-pH 6 solutions could be linked directly to the formation of bulk $(NH_4)_3[Al(OH)_6Mo_6O_{18}]$ during impregnation.

Numerous studies reported in the open literature have been dedicated to the preparation of Mo/Al_2O_3 catalyst bodies [48–55]. In most cases, the Al_2O_3 bodies were subjected to an excess of Mo solution, and the Mo complexes were applied

to the support by equilibrium adsorption processes [48–50]. These methods allow for controlled preparation in which the concentration of Mo complexes in solution never exceeds saturation values. Various Mo distribution profiles can be obtained, and the transport of Mo complexes through the Al_2O_3 bodies can even be modeled quantitatively in some cases [48]. However, the dry impregnation of support bodies, as practiced in industry, is a different process scarcely dealt with in academic studies. After incipient-wetness impregnation, the solution is forced into the pores by the capillary forces, and a highly increased concentration of metal complexes can exist near the external surface of the support bodies. The formation of the $(NH_4)_3[Al(OH)_6Mo_6O_{18}]$ precipitate is probably the result of these extreme conditions and thus likely was not observed in the studies mentioned above.

Using a staining method, a sharp Mo eggshell distribution was visually observed in Al_2O_3 pellets after dry impregnation with an AHM solution by Srinivasan et al. [55]. This may have been due to the formation of a $(NH_4)_3[Al(OH)_6Mo_6O_{18}]$ phase during impregnation, although characterization was not sufficient to support this assumption. A series of publications by Okamoto and co-workers dealt with the influence of a large number of preparation parameters, on the properties of Mo/Al_2O_3 extrudates [51–54]. A number of samples in this study were prepared by pore-volume impregnation with AHM solution of pH 5. In some of these samples, crystalline MoO_3 was observed by XRD and Raman spectroscopy performed on crushed extrudates, in agreement with the present study. However, electron probe microanalysis showed no clear accumulation of Mo on the external surface in these samples.

From the observation of bulk phases exclusively near the exterior of extrudates prepared from the highly concentrated basic AHM solution, it was concluded that their formation was the result of an eggshell distribution of Mo over the extrudates. Unfortunately, in the studies mentioned above, characterization was done only on dried material, making it difficult to discriminate between processes taking place during impregnation and those occurring during drying. The application of Raman microspectroscopy during the entire preparation process of Mo/Al_2O_3 extrudates allows us to monitor not only the distribution, but also the nature of Mo complexes in the extrudates and to envisage the processes that occur. Spectroscopy studies on crushed extrudates fail to provide this kind of information. In this way, many pitfalls related to the preparation of supported metal(oxide) catalyst bodies can be avoided.

After calcination, the amorphous nature of the supported MoO_x phase means that broad bands are generally present in the corresponding Raman spectra. In contrast, the presence of bulk material can be readily detected, because the formation of these phases yields intense and sharp peaks. This inherent sensitivity is clearly illustrated by comparing the Raman spectra recorded on calcined 19 wt% MoO_3 AHM-pH 9 extrudates (Fig. 6) with the XRD pattern recorded on the same sample (Fig. 5). Particularly when the respective accumulation times for the Raman (2 min) and XRD (14 h) measurements are taken into account, the difference in sensitivity between these techniques is striking. Because the formation of crystalline material generally should be avoided in supported catalysts, Raman (micro)spectroscopy could be an interesting technique for the development of a quality control expert system for industrial catalyst preparation processes. Although quantitative Raman spectroscopy is difficult for these inherently inhomogeneous samples, the amount of crystalline MoO_3 can be estimated, using physical mixtures as references.

4. Conclusion

Several physicochemical processes operating at different stages of the preparation process can result in poor dispersion of the Mo oxide phase in oxidic Mo/Al_2O_3 extrudates. Formation of a layer of $(NH_4)_3[Al(OH)_6Mo_6O_{18}]$ on the outer surface of the extrudates during impregnation with acidic AHM solutions occurs due to ligand-promoted dissolution of the support oxide. This leads to the formation of bulk MoO_3 after calcination. When impregnation is carried out with basic AHM solutions, a redistribution of Mo complexes during drying can lead to an eggshell distribution of Mo complexes inside the extrudates. As a result, at high Mo loadings, the Mo concentration on the outside of the extrudates exceeds the dispersion limit of the support, and MoO_3 and $Al_2(MoO_4)_3$ crystals are formed during calcination. Both phenomena are restricted to preparation of catalyst bodies and would have been overlooked in catalyst preparation studies on powdered samples. The formation of crystalline oxidic phases after calcination leads to a poorly dispersed MoS_2 phase in the active catalysts. A correlation is found between the hydrotreating activity and the dispersion of the Mo phase. Samples prepared from AHM–citrate solutions show good Mo dispersion throughout the preparation process and increased HDS activity relative to the samples.

Acknowledgments

The authors thank Dimitri Agterveld (Akzo Nobel Chemicals Research) for carrying out the SEM and TEM measurements on the MoS_2/Al_2O_3 extrudates. They acknowledge valuable discussions with Jan Nieman, EelcoVogt (Albemarle Catalysts BV), and Brenda Rossenaar (Akzo Nobel Chemicals Research). B.M.W. acknowledges financial support by the Dutch National Science Foundation (NWO-CW-van der Leeuw and VICI grants) and NRSC-Catalysis. Part of this research was sponsored by Albemarle Catalysts BV.

Supplementary material

The online version of this article contains additional supporting information.

Please visit DOI:10.1016/j.jcat.2006.07.022.

References

[1] H. Topsoe, B.S. Clausen, F.E. Massoth (Eds.), Hydrotreating Catalysis, Springer-Verlag, Berlin, 1996.
[2] A. Ishihara, F. Dumeignil, J. Lee, K. Mitsuhashi, E.W. Qian, T. Kabe, Appl. Catal. A Gen. 289 (2005) 163.
[3] D. Genuit, P. Afanasiev, M. Vrinat, J. Catal. 235 (2005) 302.

[4] H. Farag, K. Sakanishi, J. Catal. 225 (2004) 531.
[5] S.T. Oyama, J. Catal. 216 (2003) 343.
[6] S.F. Yang, R. Prins, Chem. Commun. (2005) 4178.
[7] E.J.M. Hensen, P.J. Kooyman, Y. van der Meer, A.M. van der Kraan, V.H.J. de Beer, J.A.R. van Veen, R.A. van Santen, J. Catal. 199 (2001) 224.
[8] J. Grimblot, Catal. Today 41 (1998) 111.
[9] R. Prins, Adv. Catal. 46 (2002) 399.
[10] L. Medici, R. Prins, J. Catal. 163 (1996) 38.
[11] A. Griboval, P. Blanchard, E. Payen, M. Fournier, J.L. Dubois, Catal. Today 45 (1998) 277.
[12] G. Kishan, L. Coulier, V.H.J. de Beer, J.A.R. van Veen, J.W. Niemantsverdriet, Chem. Commun. (2000) 1103.
[13] M.Y. Sun, D. Nicosia, R. Prins, Catal. Today 86 (2003) 173.
[14] S.Y. Lee, R. Aris, Catal. Rev. Sci. Eng. 27 (1985) 207.
[15] A.V. Neimark, L.I. Kheifez, V.B. Fenelonov, Ind. Eng. Chem. Prod. Res. Dev. 20 (1981) 439.
[16] G. Ertl, H. Knozinger, J. Weitkamp (Eds.), Preparation of Solid Catalysts, Wiley–VCH, Weinheim, 1999.
[17] H. Jeziorowski, H. Knözinger, J. Phys. Chem. 83 (1979) 1166.
[18] I.E. Wachs, Catal. Today 27 (1996) 437.
[19] G. Mestl, T.K.K. Srinivasan, Catal. Rev. Sci. Eng. 40 (1998) 451.
[20] J. Leyrer, D. Mey, H. Knozinger, J. Catal. 124 (1990) 349.
[21] E. Taglauer, H. Knozinger, S. Gunther, Nucl. Instrum. Methods Phys. Res. Sect. B Beam Interact. Mater. Atoms 158 (1999) 638.
[22] G. Mestl, C. Linsmeier, R. Gottschall, M. Dieterle, J. Find, D. Herein, J. Jager, Y. Uchida, R. Schlogl, J. Mol. Catal. A Chem. 162 (2000) 455.
[23] B. Pettinger, B. Ren, G. Picardi, R. Schuster, G. Ertl, Phys. Rev. Lett. 92 (2004).
[24] C. Fokas, V. Deckert, Appl. Spectrosc. 56 (2002) 192.
[25] J.A. Bergwerff, T. Visser, R.G. Leliveld, B.A. Rossenaar, K.P. de Jong, B.M. Weckhuysen, J. Am. Chem. Soc. 126 (2004) 14548.
[26] L.G. van de Water, J.A. Bergwerff, T.A. Nijhuis, K.P. de Jong, B.M. Weckhuysen, J. Am. Chem. Soc. 127 (2005) 5024.
[27] A.A. Lysova, I.V. Koptyug, R.Z. Sagdeev, V.N. Parmon, J.A. Bergwerff, B.M. Weckhuysen, J. Am. Chem. Soc. 127 (2005) 11916.
[28] H. Knözinger, E. Taglauer, in: G. Ertl, H. Knözinger, J. Weitkamp (Eds.), Preparation of Solid Catalysts, Wiley–VCH, Weinheim, 1999, p. 501.
[29] H.J. Tian, I.E. Wachs, L.E. Briand, J. Phys. Chem. B 109 (2005) 23491.
[30] T. Ozeki, H. Kihara, S. Ikeda, Anal. Chem. 60 (1988) 2055.
[31] L. Le Bihan, P. Blanchard, M. Fournier, J. Grimblot, E. Payen, J. Chem. Soc. Faraday Trans. 94 (1998) 937.
[32] X. Carrier, J.F. Lambert, M. Che, J. Am. Chem. Soc. 119 (1997) 10137.
[33] Z.H. Zhou, H.L. Wan, K.R. Tsai, Inorg. Chem. 39 (2000) 59.
[34] J.J. Cruywagen, E.A. Rohwer, G.F.S. Wessels, Polyhedron 14 (1995) 3481.
[35] X. Carrier, J.F. Lambert, S. Kuba, H. Knozinger, M. Che, J. Mol. Struct. 656 (2003) 231.
[36] G. Deo, I.E. Wachs, J. Phys. Chem. 95 (1991) 5889.
[37] H.C. Hu, I.E. Wachs, S.R. Bare, J. Phys. Chem. 99 (1995) 10897.
[38] S. Braun, L.G. Appel, V.L. Camorim, M. Schmal, J. Phys. Chem. B 104 (2000) 6584.
[39] L.M. Knijff, Ph.D. thesis, Utrecht University, 1993.
[40] A. Muller, T. Weber, Appl. Catal. 77 (1991) 243.
[41] R. Prins, A. Egorova, A. Rothlisberger, Y. Zhao, N. Sivasankar, P. Kukula, Catal. Today 111 (2006) 84.
[42] K.P. De Jong, Ind. Eng. Chem. Res. 33 (1994) 3141.
[43] S.K. Bej, A.K. Dalai, J. Adjaye, Pet. Sci. Technol. 20 (2002) 867.
[44] D. Ferdous, A.K. Dalai, J. Adjaye, Ind. Eng. Chem. Res. 45 (2006) 544.
[45] R.A. Diazreal, R.S. Mann, I.S. Sambi, Ind. Eng. Chem. Res. 32 (1993) 1354.
[46] L.G.A. van de Water, J.A. Bergwerff, B.R.G. Leliveld, B.M. Weckhuysen, K.P. de Jong, J. Phys. Chem. B 109 (2005) 14513.
[47] J.A. Bergwerff, L.G.A. van de Water, T. Visser, P. de Peinder, B.R.G. Leliveld, K.P. de Jong, B.M. Weckhuysen, Chem. Eur. J. 11 (2005) 4592.
[48] M.A. Goula, C. Kordulis, A. Lycourghiotis, J. Catal. 133 (1992) 486.
[49] M.A. Goula, C. Kordulis, A. Lycourghiotis, J.L.G. Fierro, J. Catal. 137 (1992) 285.
[50] L. Kaluza, M. Zdrazil, Catal. Lett. 78 (2002) 313.
[51] Y. Okamoto, Y. Arima, K. Nakai, S. Umeno, N. Katada, H. Yoshida, T. Tanaka, M. Yamada, Y. Akai, K. Segawa, A. Nishijima, H. Matsumoto, M. Niwa, T. Uchijima, Appl. Catal. A Gen. 170 (1998) 315.
[52] Y. Okamoto, Y. Arima, M. Hagio, K. Nakai, S. Umeno, Y. Akai, K. Uchikawa, K. Inamura, T. Ushikubo, N. Katada, S. Hasegawa, H. Yoshida, T. Tanaka, T. Isoda, I. Mochida, K. Segawa, A. Nishijima, M. Yamada, H. Matsumoto, M. Niwa, T. Uchijima, Appl. Catal. A Gen. 170 (1998) 329.
[53] Y. Okamoto, S. Umeno, Y. Arima, K. Nakai, T. Takahashi, K. Uchikawa, K. Inamura, Y. Akai, O. Chiyoda, N. Katada, T. Shishido, H. Hattori, S. Hasegawa, H. Yoshida, K. Segawa, N. Koizumi, M. Yamada, A. Nishijima, T. Kabe, A. Ishihara, T. Isoda, I. Mochida, H. Matsumoto, M. Niwa, T. Uchijima, Appl. Catal. A Gen. 170 (1998) 343.
[54] Y. Okamoto, S. Umeno, Y. Shiraki, Y. Arima, K. Nakai, O. Chiyoda, H. Yoshida, K. Uchikawa, K. Inamura, Y. Akai, S. Hasegawa, T. Shishido, H. Hattori, N. Katada, K. Segawa, N. Koizumi, M. Yamada, I. Mochida, A. Ishihara, T. Kabe, A. Nishijima, H. Matsumoto, M. Niwa, T. Uchijima, Appl. Catal. A Gen. 170 (1998) 359.
[55] R. Srinivasan, H.C. Liu, S.W. Weller, J. Catal. 57 (1979) 87.